A New Spatial Three-DoF Parallel Manipulator With High Rotational Capability

Xin-Jun Liu and Jongwon Kim

***Abstract*—This paper concerns the proposal and analysis of a novel spatial parallel manipulator. The parallel manipulator consists of a base plate, a movable platform, and three connecting legs. The moving platform has three degrees of freedom (DoFs), which are two degrees of translational freedom and one degree of rotational freedom, with respect to the base plate. The inverse and forward kinematics problems are described in closed forms and the velocity equation of the new parallel manipulator is given. Three kinds of singularities are presented. The workspace for the manipulator is analyzed systematically. Especially, the indices to evaluate the rotational capability of the moving platform of the manipulator will be defined and discussed in detail. Due to the high rotational capability performance, the proposed manipulator has wide application in the fields of industrial robots, simulators, micromotion manipulators, and parallel kinematic machines.**

***Index Terms*—Kinematics, parallel manipulators, rotational capability, singularity, workspace.**

I. Introduction

In THE PAST two decades, there have been considerable developments in the field of parallel manipulators because they can be used as industrial robots [1], simulators [2], force/torque sensors [3], micromanipulators [4], [5], and parallel kinematic machines [6].

The most studied parallel manipulators have been those with six degrees of freedom (DoFs) [7]–[10]. They have the advantages of high stiffness and the capability to handle large payloads [11], but they suffer from the problems of having a relatively small useful workspace, design difficulties, and, especially, limited rotational capability. The six-DoF parallel manipulators with high rotational capability are limited to the architectures with redundant actuators [12]. For such reasons, parallel manipulators with two and three DoFs have attracted increasing attention. For such parallel manipulators, the kinematics problems can be described in closed forms. Their design problem is relatively simpler and all possible singular configurations can be found easily. Moreover, increasing the redundant constraint will improve the stiffness of such systems. For example, the architecture that was used in the design of a parallel kinematic machine [13] is identical with that of the DELTA [16] with prismatic actuators. In DELTA, there are two bars for each leg. In the system in [13], there are three bars. The additional bar is used to improve only the stiffness. The extra bar will not affect the kinematics and workspace.

For the family of three-DoF parallel manipulators, there are many different architectures. But the most proposed three-DoF parallel manipulators are the ones that can output three planar motions [14], [15], pure translations [16], [17], [33], [34], pure rotations [18], [19], and complex DoFs [20]. Another type of three-DoF parallel manipulator is the one with a moving platform connected to the base through four legs, where the fourth leg is a passive one that determines the output of the moving platform [21]. Such parallel manipulators with high rotational capability just involve those with planar kinematics, e.g., the planar 3-RRR (R-revolute joint) parallel manipulator. The spatial three-DoF full parallel manipulator, which can combine translational and rotational DoFs with high rotational capability, needs to be researched further in the context of industrial applications.

In this paper, a new spatial three-DoF parallel manipulator is proposed. The movable platform has three DoFs, which are two translations and one rotation, with respect to the base. The kinematics problems and velocity equation of the new parallel manipulator are given. Three kinds of singularities are presented. The workspace for the manipulator is analyzed systematically; in particular, the indices that are used to evaluate the rotational capability of the moving platform will be defined and discussed in detail. The parallel manipulator studied here has wide application in the fields of industrial robots, simulators, micro-motion manipulators, and parallel kinematics machines. The kinematics, velocity, singularity, and workspace analyses presented in this paper can be useful in the design, application, and control of such devices.

II. Description of the Manipulator

A. Manipulator Structure

The new parallel manipulator, shown in Fig. 1, contains a triangular plate referred to as the moving platform. The platform is an isosceles triangle described by a parameter r, where $O'P_i = r(i = 1, 2, 3)$, as shown in Fig. 2. The vertices of this platform are connected to the base through three legs $P_iB_i(i = 1, 2, 3)$. In this paper the three legs are referred to as the first, second, and third legs, respectively. The first and second legs are in a same plane and have identical chains, each of which consists of a planar four-bar parallelogram connected to the moving platform by a revolute joint and linked to the base through an active prismatic joint. Axes of the two revolute joints

Manuscript received July 7, 2003; revised December 5, 2003. Recommended by Technical Editor M. Meng. This work was supported in part by the NRL Program on Next Generation Parallel Mechanism Platforms, by Micro-thermal System ERC, by Tsinghua Basic Research Foundation, and by the Brain Korea 21 Project.

X.-J. Liu is with the Manufacturing Engineering Institute, Department of Precision Instruments, Tsinghua University, Beijing 100084, China (e-mail: xinjunliu@mail.tsinghua.edu.cn).

J. Kim is with the Robust Design Engineering Laboratory, School of Mechanical and Aerospace Engineering, Seoul National University, Seoul, Korea (e-mail: jongkim@snu.ac.kr).

Digital Object Identifier 10.1109/TMECH.2005.856219

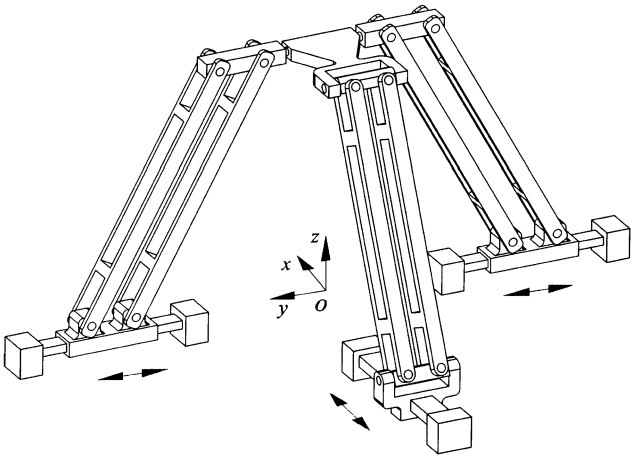

Fig. 1. The new spatial three-DoF parallel manipulator.

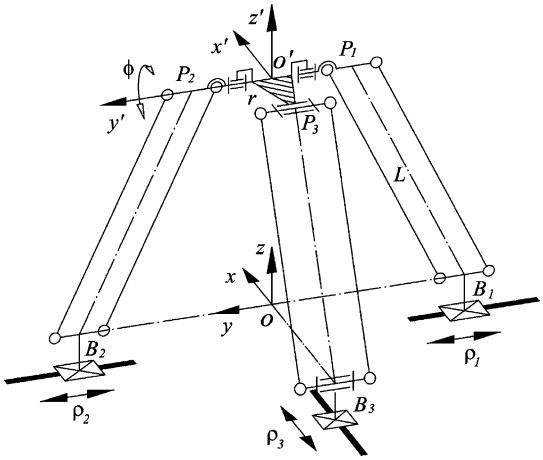

Fig. 2. A kinematics model of the manipulator.

are collinear with the y'-axis. The third leg is very different from the other two legs; it consists of another planar four-bar parallelogram that is linked to an active slider by a passive revolute joint and is connected to the moving platform through another passive revolute joint, the axis of which is parallel to the y'-axis. The slider is then attached to the base by a prismatic joint. Drives for the first and second legs are along the y-axis and along the x-axis for the third leg.

B. Manipulator Capability

The first issue to address in the design of a mechanical system is to demonstrate its capability. Due to the arrangement of the manipulator's links and joints, as shown in Figs. 1 and 2, the axes for revolute joints that connect the first and second legs to the moving platform are collinear and are parallel to that of the joint linked to the moving platform with the third leg. The first and second legs provide three constraints on the rotation of the moving platform about the x- and z-axes and on the translation along the x-axis. The third leg provides two constraints on the rotation of the moving platform about the x- and z-axes. Hence, the combination of the three legs constrains the rotation of the moving platform with respect to the x- and z-axes and the translation along the x-axis. This constraint leaves the manipulator with two translational DoFs in the O-yz plane and one rotational DoF about the y-axis. Table I shows the description. Since at every instant the rotation DoF is with respect to the collinear axes of the revolute joints connecting to the moving platform in the first and second legs, the translation along the x-axis for a reference point on the moving platform is related to the distance between the point to the collinear axis and the rotational DoF. The rotational DoF is independent. Therefore, the translation is dependent on the rotational DoF and cannot be called the DoF of the manipulator. We therefore say that the combination of the three legs can constrain the translation of the moving platform along the x-axis.

TABLE I
CONSTRAINTS AND DoF OF THE MANIPULATOR

Single leg			Combination of three legs	
No.	Chain type	Constraints	Constraints	Remained DoFs
1	$P_y(Pa)R_y$	{RO_x, RO_z, T_x }	{T_x, RO_x, RO_z}	{T_y, T_z, RO_y}
2	$P_y(Pa)R_y$	{RO_x, RO_z, T_x }		
3	$P_xR_y(Pa)R_y$	{RO_x, RO_z}		

where, P-prismatic joint, R-revolute joint, (Pa)-parallelogram, T-translation. RO-rotation, in each of which the subscript stands for the DoF.

TABLE II
POSSIBLE CHAINS FOR LEGS AND THE MANIPULATOR

Leg chain			Manipulator chains
First leg	Second leg	Third leg	
$P_y(Pa)R_y$	$P_y(Pa)R_y$	$P_xR_y(Pa)R_y$	$P_y(Pa)R_y$- $P_y(Pa)R_y$- $P_xR_y(Pa)R_y$
			$P_y(Pa)R_y$- $P_yR_xU_{xy}$- $P_xR_y(Pa)R_y$
		P_xUU	$P_y(Pa)R_y$- $P_y(Pa)R_y$- P_xUU
	$P_yR_xU_{xy}$		$P_y(Pa)R_y$- $P_yR_xU_{xy}$- P_xUU
		P_xUS (or P_xSS)	$P_y(Pa)R_y$- $P_y(Pa)R_y$- P_xUS
			$P_y(Pa)R_y$- $P_yR_xU_{xy}$- P_xUS

where, P-prismatic joint, R-revolute joint, U-universal joint, (Pa)-parallelogram, S-spherical joint, in each of which the subscript stands for the DoF.

From Table I, we can see that the first leg itself can constrain the moving platform with the translation along the x-axis and rotations about the z- and x-axes. The second leg chain can be identical with or different from the first leg; e.g., the second leg can be with a $P_yR_xU_{xy}$ chain. The combination of the first and second legs can also provide the manipulator with the same constraints, i.e., the translation along the x-axis and rotations about the z- and x-axes. More important, the third leg can then be a four-DoF, five-DoF, or six-DoF chain, e.g., a P_xUU or P_xUS. It can also be a traditional P_xSS chain. The possible chains for the three legs and the manipulator are shown in Table II, where one can see that there are six types of manipulators with

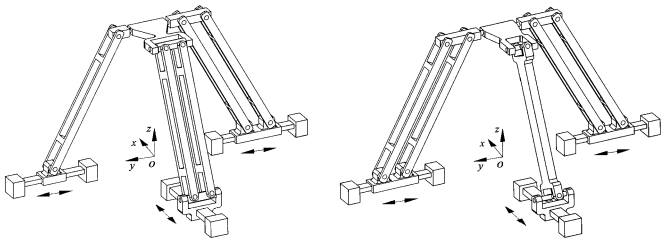

Fig. 3. Two kinds of topology architectures.

different leg chains; e.g., manipulators with $\mathrm{P_y(Pa)R_y\text{-}P_yR_x}$ $\mathrm{U_{xy}\text{-}P_xR_y(Pa)R_y}$ and $\mathrm{P_y(Pa)R_y\text{-}P_y(Pa)R_y\text{-}P_xUU}$ chains are shown in Fig. 3(a) and (b), respectively. To note, in the $\mathrm{P_xUU}$ chain, the axis of the revolute joint in the first U joint that is attached to the P joint must be parallel to the y-axis, and the axis of the revolute joint in the second U joint that is connected to the moving platform must also be parallel to the y-axis. Then the manipulators can also have three DoFs. Additionally, for the $\mathrm{P_xUS}$ chain in Table II, the axis of the revolute joint in the first U joint that is attached to the P joint should be parallel to the y-axis as well.

C. Novelties and Applications

This paper concerns the architecture shown in Fig. 1, which we prefer for the following reasons: 1) the identical chains for the first and second legs can increase the system's stiffness and symmetry and 2) all joints in the architecture, being single-DoF joints, can improve the rotational capability of the moving platform. The U and S joints will limit the manipulator's rotational capability for the limited motion range. Many are interested in the novel parallel structure of the manipulator as it may be applicable in mechanical design and practical applications. The mechanical design of the manipulator is interesting because the concept of the leg mechanisms was conceived on the basis of a planar four-bar parallelogram, which has been used in the design of other parallel manipulators, such as Star Like robot [17], Tsai's manipulator [22], CaPaMan [23], Orthoglide [33], etc. The novelties of the new spatial three-DoF parallel manipulator are as follows: The combining of the spatial translational and rotational DoFs in a spatial three-DoF system; only single-DoF joints; and high rotational capability of the rotational DoF, which will be illustrated in the Workspace Analysis and Example sections.

The practical application can be advanced to the parallel kinematic machine [6], which has become more attractive since 1994, and any other manipulating devices. Because of the low rotational capability and flexibility of six-DoF parallel manipulators, more and more parallel kinematic machines are built as hybrid structures, which are usually based on the parallel manipulators with two or three DoFs [21], [24]. Another advantage from designing a machine tool based on a two- or three-DoF parallel manipulator is the improvement in stiffness due to more use of redundant constraints. The parallel manipulator proposed in this paper can also be designed as a hybrid parallel kinematic machine. And we believe that the parallel manipulator can also be used as an industrial robot and a motion simulator.

III. Kinematics Problems of the Manipulator

A. Inverse Kinematics

The inverse kinematics problem involves mapping a known pose (position and orientation) of the output platform of the manipulator to a set of input joint variables that will achieve that pose. A kinematics model of the manipulator is developed as shown in Fig. 2. Vertices of the output platform are denoted as platform joints $P_i (i = 1, 2, 3)$, and vertices of the base joints are denoted as $B_i (i = 1, 2, 3)$. A fixed global reference system $\Re$:O-xyz is located at the point of intersection between B_1B_2 and OB_3 with the z-axis normal to the plane $B_1B_2B_3$ and the y-axis directed along B_1B_2. Another reference frame, called the top frame $\Re'$:O'-$x'y'z'$, is located at the center of the side P_1P_2. The z'-axis is perpendicular to the output platform and the y'-axis is directed along P_1P_2. The link length for each leg is denoted as L, where $P_iB_i = L, i = 1, 2, 3$.

For inverse kinematics analysis, the pose of the moving platform is considered known, the position is given by the position vector $(\boldsymbol{O'})_{\Re}$, and the orientation is given by matrix $\boldsymbol{Q}$ and there is

$$(\boldsymbol{O'})_{\Re} = (x\ y\ z)^{\mathrm{T}} \tag{1}$$

where $x = 0$, and

$$\boldsymbol{Q} = \begin{bmatrix} \cos\phi & 0 & \sin\phi \\ 0 & 1 & 0 \\ -\sin\phi & 0 & \cos\phi \end{bmatrix} \tag{2}$$

where the angle ϕ is the rotational DoF of the output platform with respect to the collinear axes of the revolute joints connected to the moving platform in the first and second legs, as shown in Fig. 2. The inverse kinematics of the parallel manipulator can be solved by writing the following constraint equation:

$$\|[\boldsymbol{p}_i - \boldsymbol{b}_i]_{\Re}\| = L, \qquad i = 1, 2, 3 \tag{3}$$

where vectors $(\boldsymbol{b}_i)_{\Re}$ and $(\boldsymbol{p}_i)_{\Re} (i = 1, 2, 3)$ are position vectors of joints B_i and P_i in frame $\Re$, respectively, and

$$(\boldsymbol{p}_i)_{\Re} = \boldsymbol{Q}(\boldsymbol{p}_i)_{\Re'} + (\boldsymbol{O'})_{\Re} \tag{4}$$

in which $(\boldsymbol{p}_i)_{\Re'} (i = 1, 2, 3)$ are the vectors of joints P_i in frame $\Re'$. Hence, for a given manipulator and for prescribed values of the position and orientation of the platform, the required actuator inputs can be directly computed from (3); that is,

$$\rho_1 = \pm\sqrt{L^2 - z^2} + y - r \tag{5}$$

$$\rho_2 = \pm\sqrt{L^2 - z^2} + y + r \tag{6}$$

$$\rho_3 = \pm\sqrt{L^2 - (z + r\sin\phi)^2 - y^2} - r\cos\phi. \tag{7}$$

From (5)–(7), one can see that there are eight inverse kinematics solutions for a given pose of the parallel manipulator. To obtain the inverse configuration as shown in Fig. 1, the sign "±" in each of (5) and (7) should be "—" and that of (6) should be "+". Actually, the same sign in (5) and (6) will lead to

singularity, which will be discussed in the Singularity Analysis section. Therefore, there are only four inverse kinematics solutions.

B. Forward Kinematics

The objective of the forward kinematics solution is to define a mapping from a known set of the actuated inputs to an unknown pose of the moving platform. For the architecture with prismatic actuators, as shown in Fig. 2, the inputs that are considered to be known are ρ_1, ρ_2, and ρ_3. The unknown pose of the moving platform is described by the position vector $[\boldsymbol{O}']_{\Re}$ and the angle ϕ. Since the signs "$\pm$" in (5) and (6) should be different, (5) plus (6) leads to

$$y = (\rho_1 + \rho_2)/2. \tag{8}$$

Substitution into (6) leads to

$$z = \pm\sqrt{L^2 - [r + (\rho_1 - \rho_2)/2]^2}. \tag{9}$$

If z and y are obtained from (8) and (9), the direct solutions of angle ϕ can be reached from (7) as

$$\phi = 2\ \tan^{-1}(t) \tag{10}$$

where

$$t = (A \pm \sqrt{A^2 + B^2 - C^2})/(B - C) \tag{11}$$

with $A = 2zr, B = 2r\rho_3$, and $C = y^2 + \rho_3^2 + z^2 + r^2 - L^2$.

From (8)–(11), we can see that for the given values of ρ_1, ρ_2, and ρ_3, there are one solution for y, two solutions for z, and four solutions for ϕ. Then, there are four forward kinematics solutions. To obtain the forward configuration as shown in Fig. 1, the sign "$\pm$" in (9) should be "+" and that in (11) should be "$-$."

IV. Velocity Equations

Equation (3) can be differentiated with respect to time to obtain the velocity equations, which leads to

$$(y - r - \rho_1)\dot{\rho}_1 = (y - r - \rho_1)\dot{y} + z\dot{z} \tag{12}$$

$$(y + r - \rho_2)\dot{\rho}_2 = (y + r - \rho_2)\dot{y} + z\dot{z} \tag{13}$$

$$-(r\cos\phi + \rho_3)\dot{\rho}_3 = y\,\dot{y} + (r\sin\phi + z)\dot{z} + [rz\cos\phi - r\rho_3\sin\phi]\dot{\phi}. \tag{14}$$

Rearranging (12)–(14) leads to an equation of the form

$$\boldsymbol{A}\dot{\boldsymbol{\rho}} = \boldsymbol{B}\dot{\boldsymbol{p}} \tag{15}$$

where $\dot{\boldsymbol{p}}$ is the vector of output velocities defined as

$$\dot{\boldsymbol{p}} = (\dot{y}\ \dot{z}\ \dot{\phi})^{\mathrm{T}} \tag{16}$$

and $\dot{\boldsymbol{\rho}}$ is the vector of input velocities defined as

$$\dot{\boldsymbol{\rho}} = (\dot{\rho}_1\ \dot{\rho}_2\ \dot{\rho}_3)^{\mathrm{T}}. \tag{17}$$

Matrices $\boldsymbol{A}$ and $\boldsymbol{B}$ can be expressed as

$$\boldsymbol{A} = \begin{bmatrix} y - r - \rho_1 & 0 & 0 \\ 0 & y + r - \rho_2 & 0 \\ 0 & 0 & -(r\cos\phi + \rho_3) \end{bmatrix} \tag{18}$$

$$\boldsymbol{B} = \begin{bmatrix} y - r - \rho_1 & z & 0 \\ y + r - \rho_2 & z & 0 \\ y & r\sin\phi + z & rz\cos\phi - \rho_3 r\sin\phi \end{bmatrix}. \tag{19}$$

The Jacobian matrix of the manipulator can be written as

$$\boldsymbol{J} = \boldsymbol{A}^{-1}\boldsymbol{B}. \tag{20}$$

V. Singularity Analysis

In the parallel manipulator, singularities occur whenever $\boldsymbol{A}, \boldsymbol{B}$, or both become singular. As singularity leads to a loss of the controllability and degradation of the natural stiffness of manipulators, the analysis of parallel manipulators has drawn considerable attention [25], [26], [35], [36]. Based on the matrices $\boldsymbol{A}$ and $\boldsymbol{B}$, a classification of the singularities pertaining to parallel manipulators into three main groups was suggested [26].

From (18) and (19), $\det(\boldsymbol{A}) = 0$ and $\det(\boldsymbol{B}) = 0$ lead to

$$(y - r - \rho_1)(y + r - \rho_2)(r\cos\phi + \rho_3) = 0 \tag{21}$$

and

$$zr(z\cos\phi - \rho_3\sin\phi)(\rho_2 - \rho_1 - 2r) = 0 \tag{22}$$

respectively.

From (21), one obtains

$$y - r - \rho_1 = 0 \tag{23}$$

or

$$y + r - \rho_2 = 0 \tag{24}$$

or

$$r\cos\phi + \rho_3 = 0 \tag{25}$$

that is, $\det(\boldsymbol{A}) = 0$ occurs whenever one of the three following cases arises: (1) the leg P_1B_1 is normal to the O-xy plane, (2) P_2B_2 is normal to the O-xy plane, or (3) P_3B_3 is normal to the x-axis. If $y - r - \rho_1 = 0$, from (5) and (6), it is simple to find $y + r - \rho_2 = 0$; then (5) minus (6) yields $\rho_2 - \rho_1 - 2r = 0$, which leads to $\det(\boldsymbol{B}) = 0$ and, if $\rho_2 - \rho_1 - 2r = 0$, which means $\det(\boldsymbol{B}) = 0$, the manipulator will be in the configuration in which the first and second legs are parallel to each other, i.e., $P_1B_1 // P_2B_2$. Especially, the case in which both of the two legs are normal to the O-xy plane will also lead to $\det(\boldsymbol{A}) = 0$.

A. First Kind of Singularity

The first kind of singularity occurs when $\boldsymbol{A}$ becomes singular but $\boldsymbol{b}$ is invertible, i.e.,

$$\det(\boldsymbol{A}) = 0 \quad \text{and} \quad \det(\boldsymbol{B}) \neq 0. \tag{26}$$

This kind of singularity corresponds to the configuration in which the chain reaches either a boundary of its workspace or an internal boundary, limiting the different subregions of the workspace where the number of branches is not the same.

For the new parallel manipulator, as any configuration of the first and second legs being normal to the O-xy plane, i.e., $y - r - \rho_1 = 0$ or $y + r - \rho_2 = 0$, will also result in $\det(\boldsymbol{B}) =$

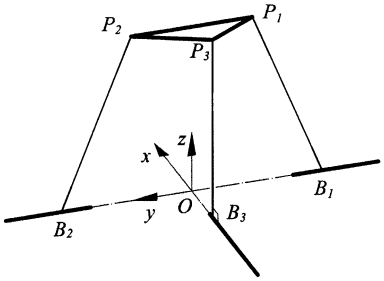

Fig. 4. One example of the first kind of singularity: $P_3B_3 \perp Ox$.

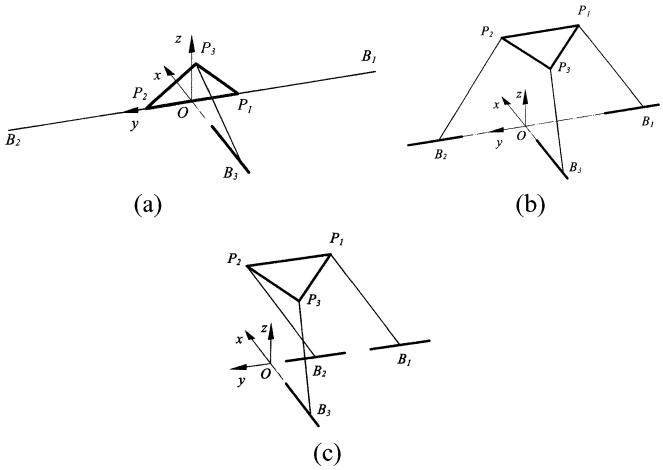

Fig. 5. Three singular configurations of the second kind of singularity. (a) P_1B_1 and P_2B_2 are in the plane O-xy. (b) P_3B_3 is in the moving platform plane. (c) $P_1B_1//P_2B_2$ but neither P_1B_1 nor P_2B_2 is normal to the O-xy plane and no $P_3B_3 \perp Ox$.

0, this kind of singularity occurs in the configuration in which only the third leg is normal to the x-axis, as shown in Fig. 4.

B. Second Kind of Singularity

The second kind of singularity, occurring only in closed kinematics chains, arises when $\boldsymbol{B}$ becomes singular but $\boldsymbol{A}$ is invertible, i.e., when

$$\det(\boldsymbol{A}) \neq 0 \quad \text{and} \quad \det(\boldsymbol{B}) = 0. \tag{27}$$

In such configuration, the output link is locally movable even when all the actuated joints are locked, and the output link cannot resist one or more forces or moments even when all actuators are locked. From (22), we can obtain the following.

- If $z = 0$, the manipulator is in the configuration in which the first and second legs are in the plane O-xy, as shown in Fig. 5(a); in such configuration, the manipulator is in its second kind of singularity.
- $r = 0$ also results in the second kind of singularity. When $z\cos\phi - \rho_3 \sin\phi = 0$ is satisfied, one obtains

$$\tan\phi = z/\rho_3. \tag{28}$$

This relation corresponds to the configuration in which the third leg P_3B_3 is in the plane defined by platform joints P_1, P_2, and P_3 (in this paper, the plane is called the moving platform plane), as shown in Fig. 5(b).

- The configuration that $P_1B_1//P_2B_2$ but neither P_1B_1 nor P_2B_2 is normal to the O-xy plane and P_3B_3 is not normal to Ox is also the kind of singularity, as shown Fig. 5(c). This is why there are four inverse kinematics solutions.
- The configuration in which both P_1B_1 and P_2B_2 are normal to the O-xy plane does not belong to the second kind of singularity since it leads to $\det(\boldsymbol{A}) = 0$ and $\det(\boldsymbol{B}) = 0$.

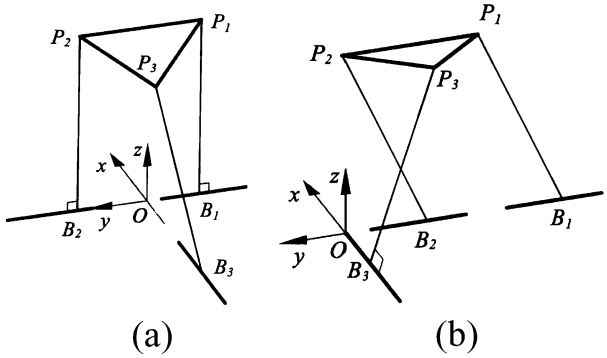

Fig. 6. Two singular configurations of the third kind of singularity. (a) Both P_1B_1 and P_2B_2 are normal to the O-xy plane. (b) $P_1B_1//P_2B_2$ and $P_3B_3 \perp Ox$.

C. Third Kind of Singularity

The third kind of singularity occurs when both $\boldsymbol{A}$ and $\boldsymbol{B}$ become simultaneously singular. This situation corresponds to configurations in which the chain can undergo finite motions when its actuators are locked or in which a finite motion of the inputs produces no motion of the output. From the above analysis, one can see that when both the first and the second legs are normal to the O-xy plane, the third kind of singularity will occur as shown in Fig. 6(a). In such a configuration, the moving platform can translate in the O-xy plane while all inputs are locked. $P_1B_1//P_2B_2$ and $P_3B_3 \perp Ox$ also result in the singularity as shown in Fig. 6(b). In such a configuration, the inputs will result in no output. If $r = 0$ and $\rho_3 = 0$, both $\det(\boldsymbol{A}) = 0$ and $\det(\boldsymbol{B}) = 0$ will be equal to zero, which leads to the singularity as well. In that case, the three legs are in the same plane, i.e., the O-yz plane. Therefore, there exists the translation in the O-yz plane, whereas inputs remain at rest.

VI. Workspace Analysis

In this section, the workspace of the proposed manipulator will be discussed systematically. Indices to evaluate the rotational capability, the gross rotational capability index (GRCI), and the net rotational capability index (NRCI) of the moving platform of the manipulator will be defined.

A. Constant Orientation Workspace

The constant orientation workspace is defined as the region that can be reached by the reference point on the moving

platform when the orientation of the moving platform is kept constant. Most research of the issue is focused on six-DoF Stewart parallel manipulators [27], [28]. The definition and more detailed research for the constant orientation workspace were presented by Merlet [29], [37]. In this paper, the workspace will be discussed first.

From (5)–(7), we can obtain

$$[y-(r+\rho_1)]^2+z^2=L^2 \tag{29}$$

$$[y-(\rho_2-r)]^2+z^2=L^2 \tag{30}$$

$$y^2+[z-(-r\sin\phi)]^2=L^2-(\rho_3+r\cos\phi)^2 \tag{31}$$

from which we can see that if ρ_1,ρ_2,ρ_3, and ϕ are specified, (29)–(31) represent three circles in the frame O-yz. For the first leg, the circle is centered at $(r+\rho_1,0)$ and the radius is L. For the second leg, the circle is centered at $(\rho_2-r,0)$ and the radius is L. And the third one, $(0,-r\sin\phi)$ and $\sqrt{L^2-(\rho_3+r\cos\phi)^2}$, are the center and radius of the circle, respectively. Indeed, if mechanical interference is neglected, the boundary of the workspace for each leg is attained whenever at least one of the actuators reaches one of its limits. If we assume that ϕ is specified and the range of motion of the actuators is given by

$$\begin{aligned}&\rho_1\in[\rho_{1\min}\rho_{1\max}]\\&\rho_2\in[\rho_{2\min},\rho_{2\max}]\\&\rho_3\in[\rho_{3\min},\rho_{3\max}],\\&\rho_{1\max}=\rho_{3\max}=-\rho_{2\min},\quad \rho_{1\min}=\rho_{3\min}=-\rho_{2\max}\end{aligned} \tag{32}$$

the workspace for each leg is the enveloping face of innumerable circles, which are denoted as Ω_1,Ω_2, and $\Omega_{3-\phi}$, respectively. The constant orientation workspace of the parallel manipulator is the intersection of the three enveloping faces.

B. The Reachable Workspace

The reachable workspace, Ω_R, is known as the region that can be reached by the reference point with at least one orientation. For the parallel manipulator studied in this paper, if the reference point $O'(y,z)$ within the intersection of the above-mentioned enveloping faces belongs to the reachable workspace, (y,z) must satisfy (31) for at least one value of $\phi\in[0,2\pi]$.

For the parallel manipulator studied here, the rotational DoF is the rotation of the moving platform with respect to the y-axis. The orientation of the moving platform does not affect the workspaces of the first and second legs. From above analysis, we can see that the reachable workspaces for the first and second legs are also the enveloping faces of innumerable circles centered at the line segments $y=r+\rho_1(\rho_1\in[\rho_{1\min},\rho_{1\max}])$ and $y=\rho_2-r(\rho_2\in[\rho_{2\min},\rho_{2\max}])$, respectively. And the radius of each circle is L.

If $\rho_1=\rho_{1\max}$ and $\rho_2=\rho_{2\min}$, (29) and (30) can be rewritten as

$$[y-(r+\rho_{1\max})]^2+z^2=L^2 \tag{33}$$

$$[y-(\rho_{2\min}-r)]^2+z^2=L^2. \tag{34}$$

If $|\rho_{1\max}|=\rho_{2\min}\geq r$, intersecting points of the above two circles can be written in the frame O-yz as

$$(0,\pm\sqrt{L^2-(\rho_{2\min}-r)^2}). \tag{35}$$

If $\rho_1=\rho_{1\min}$ and $\rho_2=\rho_{2\max}$, intersecting points of the two circles can also be obtained from (29) and (31) as

$$(0,\pm\sqrt{L^2-(\rho_{2\max}-r)^2}). \tag{36}$$

Let's consider the third leg of the manipulator. When $\phi=0$, (31) can be rewritten as

$$y^2+z^2=L^2-(\rho_3+r)^2. \tag{37}$$

Let $\rho_3\in[\rho_{3\min},\rho_{3\max}]$, the constant orientation workspace Ω_{3-0} of the leg, be the enveloping face of innumerable circles centered at the point $(y=0,z=0)$. The radius of each circle is $\sqrt{L^2-(\rho_3+r)^2}$ with $\rho_3\in[\rho_{3\min},\rho_{3\max}]$. If $y=0$ and $\rho_3=\rho_{3\min}$, from (37) one obtains

$$z=\pm\sqrt{L^2-(\rho_{3\min}+r)^2}. \tag{38}$$

If $y=0$ and $\rho_3=\rho_{3\max}$, there is

$$z=\pm\sqrt{L^2-(\rho_{3\max}+r)^2}. \tag{39}$$

Since $\rho_{1\max}=\rho_{3\max}=-\rho_{2\min}$ and $\rho_{1\min}=\rho_{3\min}=-\rho_{2\max}$, from (35), (36), (38), and (39), we can see that the constant orientation workspace $\Omega_{3-0}(\phi=0)$ of the third leg embodies the intersection of reachable workspaces of the first and second legs. Therefore, we can conclude that the intersection of reachable workspaces of the first and second legs is then the reachable workspace of the parallel manipulator when $|\rho_{1\max}|=|\rho_{3\max}|=\rho_{2\min}\geq r$.

C. Rotational Capability of the Moving Platform

Rotational capability is an index to evaluate whether a device is competent for the task in hand. One of the disadvantages of the parallel manipulator is its lower rotational capability [11], [30], which limits its further application in the industry. The analysis of rotational capability of the output link (the moving platform) in the workspace is one of the most important issues in the design and application of parallel kinematics [31], [32]. In fact, few authors addressed the issue about the evaluation of rotational capability for a parallel manipulator [38]. In [38], the authors presented the optimal design of a parallel manipulator for the given rotational capability. Here, the evaluation of rotational capability for the proposed manipulator will be investigated. According to the kinematics of our parallel manipulator, the rotational DoF is the rotation of the moving platform with respect to the y-axis as shown in Fig. 1. The position vector of point P_3 in frame $\Re$ can be written as

$$(\boldsymbol{p}_3)_{\Re}=(-r\cos\phi\quad y\quad r\sin\phi+z)^{\mathrm{T}}. \tag{40}$$

Let $x_p=-r\cos\phi, y_p=y,$ and $z_p=r\sin\phi+z$; (31) can be rewritten as

$$(x_p-\rho_3)^2+y_p^2+z_p^2=L^2 \tag{41}$$

which stands for a spherical surface centered at $(\rho_3,0,0)$, and the radius is L. If the range of motion ρ_3 of the third actuator is

specified and the workspace point (y, z) is given, (41) represents a circle centered at point $(x = \rho_3, z = 0)$, and the radius is $\sqrt{L^2 - y_p^2}$. The circle equation can be rewritten as

$$(x_p - \rho_3)^2 + z_p^2 = L^2 - y_p^2 \tag{42}$$

which is located in a plane parallel to the O-xz plane. As we know, for a given position (y, z) of the moving platform, the locus of the joint point P_3 is the subset of a circle with radius r, where the circle is denoted as ν. The equation can be written as

$$x_p^2 + (z_p - z)^2 = r^2 \tag{43}$$

which is located in the plane parallel to the O-xz plane defined by y. From (42) and (43), we can see that all the circles defined by (42) and (43) are located on the same plane. When (y, z) and ρ_3 are specified, the point of intersection (x_p, y_p, z_p) of the two circles can be obtained.

Actually, (42) represents the locus of point P_3 on the third leg when (y, z) is given. The locus that is a region is denoted as Ω_3. Then the arc of ν that lies within Ω_3 is actually the locus of point P_3 on the moving platform at point (y, z). The arc can be identified by four points, which are the intersecting points between circle ν and two circles given by (42) with $\rho_3 = \rho_{3\min}$ and $\rho_3 = \rho_{3\max}$. In this paper, the circle of (42) with $\rho_3 = \rho_{3\min}$ is denoted as $C_{3\min}$ and that with $\rho_3 = \rho_{3\max}$ is denoted as $C_{3\max}$. We can obtain the intersecting points as following.

Equation (41) minus (43) produces

$$z_p = ax_p + b \tag{44}$$

where $a = \rho_3/z$ and $b = (L^2 - y_p^2 - r^2 + z^2 - \rho_3^2)/(2z)$. Substituting (44) into (43) leads to

$$A'x_p^2 + B'x_p + C' = 0 \tag{45}$$

where $A' = 1 + a^2, B' = 2a(b - z)$, and $C' = (b - z)^2 - r^2$. Then, there is

$$x_p = (-B' \pm \sqrt{B'^2 - 4A'C'})/2A'. \tag{46}$$

z_p can be obtained by substituting (46) into (44). From (44) and (46), we can see that there are two intersecting points for each ρ_3. If $\rho_3 = \rho_{3\min}$ and $\rho_3 = \rho_{3\max}$, respectively, the maximum number of intersecting points can reach four. Then in the workspace, for a given point (y, z), the intersection between circle ν and $C_{3\min}$ and $C_{3\max}$ can be classified into four cases: a) one (two) intersecting point(s) between ν and $C_{3\max}$ and no intersection between ν and $C_{3\min}$; b) one (two) intersecting point(s) between ν and $C_{3\max}$ and one (two) intersecting point(s) between ν and $C_{3\min}$; c) no intersection between ν and $C_{3\min}$ and $C_{3\max}$. In this case, ν is embodied completely within Ω_3; and d) no intersection between ν and $C_{3\max}$, one (two) intersecting point(s) between ν and $C_{3\min}$. Based on the intersecting points, one can get the arc(s) embodied within Ω_3. The central angle of the arc(s) is defined as the gross rotational capability index ζ, which is used to evaluate the rotational capability of the moving platform at a given position (y, z) globally.

For example, as shown in Fig. 7, Ω_R is supposed to be the reachable workspace of a manipulator. The projection of the workspace to the O-xz plane is shown as line W_aW_b. The radii of two circles $C_{3\min}$ and $C_{3\max}$ are related to the value of y. If the center of circle ν changes from point W_a to W_b, the intersecting situation between ν and $C_{3\min}$ and $C_{3\max}$ will be different. For example, when ν is at the position of 1, there are two intersecting points between ν and $C_{3\max}$ but no intersection between ν and $C_{3\min}$. The value of the GRCI ζ is determined by the central angle of the arc embodied within Ω_3. When ν is located at the position of 2, where ν is centered at point W_o and the length between W_o and $(\rho_{3\min}, 0, 0)$ is $\sqrt{L^2 - y^2} + r$, there are two intersecting points between ν and $C_{3\max}$ and one intersecting point between ν and $C_{3\min}$. The three points divide the arc that is embodied within Ω_3 into two subarcs. When ν moves to the position of 3, there are four intersecting points, which means that there are two inaccessible arcs within region Ω_3. In these two cases, ζ can only be valued by the central angle of one of the two arcs. The final is the case in which ν is at the position of 4, where there are two intersections between ν and $C_{3\min}$ but no intersection between ν and $C_{3\max}$. From Fig. 7 we can see that, mostly, the circle ν is centered at line W_aW_o. Cases 2, 3, and 4 can occur only when ν is located at line W_oW_b, which is shorter than W_aW_o. More important, the workspace region in which W_oW_b corresponds in the O-yz plane is the protuberant region of the workspace. Practically, this region is not used.

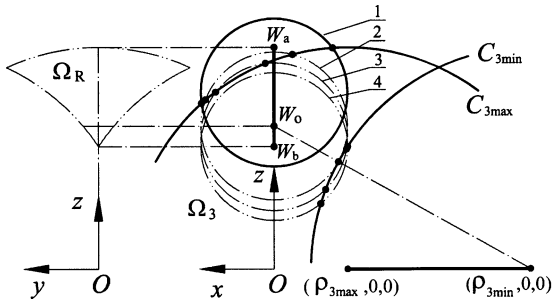

Fig. 7. Intersection classification between circle ν and $C_{3\min}$ and $C_{3\max}$.

The central angle given by the value of ζ represents the capability that the moving platform can rotate at a given point in the workspace. Note that these configurations include singularities, which will separate the arc into several manipulator-inaccessible ones. According to the analysis in Section V, what should be considered here is the singularity of the third leg B_3P_3. In Fig. 7, for cases 1 and 2, the singular configuration occurs when B_3P_3 and the moving platform are completely extended in the same plane, especially, in case 2, the singular configuration occurs when the reference point O' and the joint point B_3 are at W_o and $(\rho_{3\min}, 0, 0)$, respectively. In case 4, the singularity occurs when B_3P_3 and the moving platform are completely folded in the same plane. There is no singularity in case 3. The rotational capability of a real manipulator device can be valued by only one of the arcs, which will be defined as the NRCI ς. In fact, central angle values of the arcs correspond to different ς for the manipulators with different assembling modes. The modes can be obtained by inverse or forward kinematics solutions. For the rotational DoF, this only relates to the assembling mode of the

third leg. From (7) and (10), one can see that the third leg has two kinds of assembling modes, which is believed to have only two manipulator-inaccessible arcs. Which arc will be selected to evaluate the ς index should be determined by which assembling mode one selects.

The rotational capability formula can be found for the manipulator with the assembling mode as shown in Fig. 1, i.e., the configuration when the sign "$\pm$" in (7) is "—". If there are intersecting points between ν and $C_{3\max}$, one of which that $|x|$ is larger is denoted as $P_{\nu\max}(P_{\nu\max\_x}, P_{\nu\max\_z})$. $P_{\nu\min}(P_{\nu\min\_x}, P_{\nu\min\_z})$ specifies one of the intersecting points, if there are, between ν and $C_{3\min}$ that $|x|$ is larger. These points can be obtained from (44) and (46). Although there may exist several intersecting points between ν and $C_{3\min}$ and $C_{3\max}$, from the above analysis, we can see that the rotational capability index just depends on points $P_{\nu\max}$ and $P_{\nu\min}$ and the singular configurations. Conditions for the manipulator in singular configurations are

$$B_3c' = r + \sqrt{L^2 - y^2} \quad \text{and} \quad B_3c' = \sqrt{L^2 - y^2} \tag{47}$$

where c' is the projection in the O-xz plane of point c and $B_3c' = \sqrt{\rho_3^2 + z^2}$. The conditions correspond to singular configurations in which the third leg is in the moving platform plane. Then the net rotational capability ς of the manipulator at any point $c(y, z)$ within the workspace can be expressed as

- $\varsigma = 180^\circ$, if there is no intersecting point between ν and $C_{3\min}$ and $C_{3\max}$;
- $\varsigma = 180^\circ + \tan^{-1}[P_{\nu\max\_x}/(P_{\nu\max\_z} - z)] - \tan^{-1}(\sqrt{L^2 - y^2 - z^2}/z)$, if there is an intersecting point between ν and $C_{3\max}$ and no intersecting point between ν and $C_{3\min}$;
- $\varsigma = 180^\circ + \tan^{-1}[P_{\nu\max\_x}/(P_{\nu\max\_z} - z)] - \tan^{-1}[-P_{\nu\min\_x}/(z - P_{\nu\min\_z})]$, if there are intersecting points both between ν and $C_{3\max}$ and ν and $C_{3\min}$;
- $\varsigma = 180^\circ + \tan^{-1}[\sqrt{L^2 - y^2 - z^2}/z] - \tan^{-1}[-P_{\nu\min\_x}/(z - P_{\nu\min\_z})]$, if there is no intersecting point between ν and $C_{3\max}$, but there is between ν and $C_{3\min}$

from which we can see that the rotational capability cannot be larger than 180° because of the singularity problem. Similarly, the NRCI formula for the manipulator with the assembling mode when the sign "$\pm$" in (7) is "+" can be obtained as well, but will not be discussed here.

VII. Example

An example of an application of the analysis for the parallel manipulator proposed in this paper, the kinematics problems, singularity, and workspace of a manipulator, where $r = 1.0$ and $L = 3.0$, are considered in this section.

As discussed in Section III, there are, respectively, four solutions for the inverse and forward kinematics problems of the parallel manipulator. The corresponding configurations are shown in Figs. 8 and 9, respectively. For this example, the position and orientation of the manipulator for the inverse kinematics are $y = 0.8, z = 2.5$ and $\phi = 15^\circ$. And the inputs for the forward kinematics are $\rho_1 = -1.8, \rho_2 = 2.2$, and $\rho_3 = -1.8$, respectively.

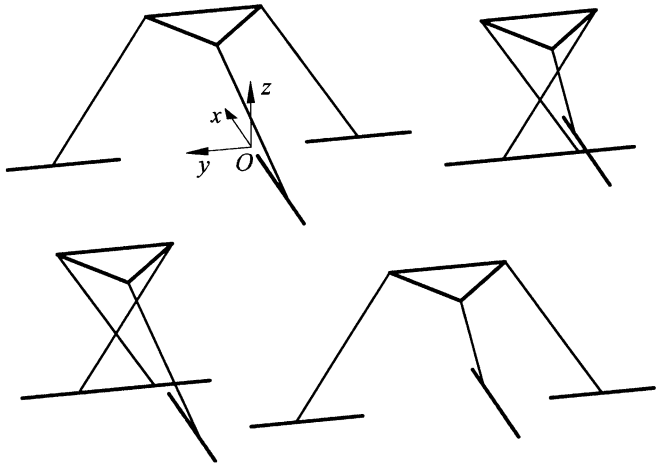

Fig. 8. Four inverse kinematics solutions.

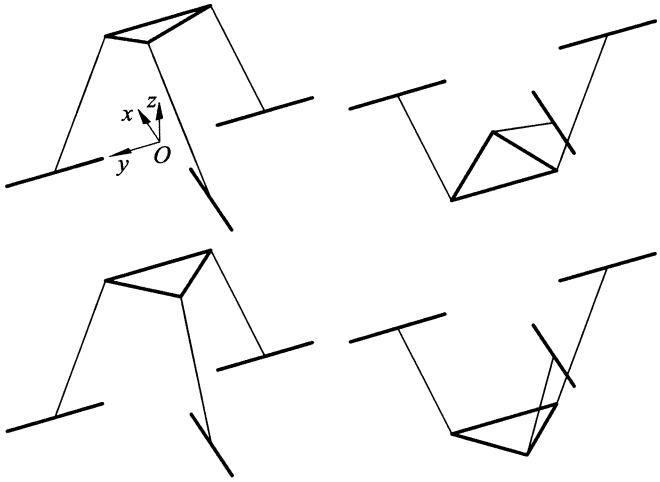

Fig. 9. Four forward kinematics solutions.

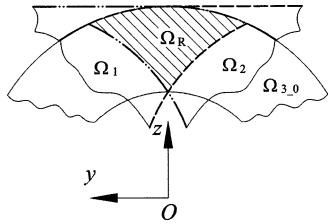

Fig. 10. Reachable workspace Ω_R.

In order to analyze the workspace, the actuated motions are specified as

$$\rho_1, \rho_3 \in [-3.5, -1.0] \quad \rho_2 \in [1.0, 3.5]. \tag{48}$$

According to the analysis of the workspace in Section VI(B), the reachable workspace of the example is the shaded region Ω_R in Fig. 10, which is the intersection of the workspaces of the first and second legs. The workspace of the first leg is the region between the boundaries shown as the dashed arcs in Fig. 10, and the workspace for the second leg is the region between the

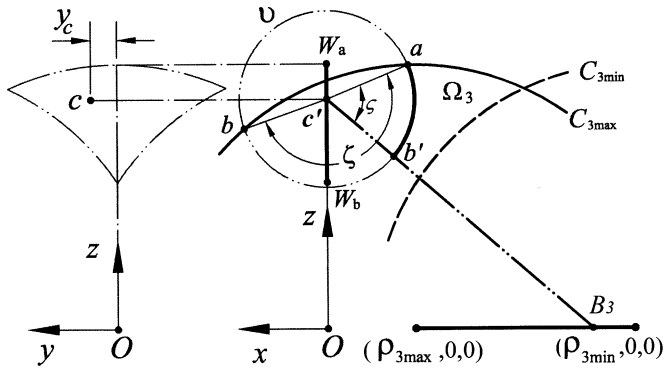

Fig. 11. Rotational capability analysis example.

long-dash double-dot arc boundaries. To prove the results of Section VI-B, the orientation workspace of the third leg when $\phi = 0$ is also illustrated in Fig. 10, which is region Ω_{3-0} between the solid arc boundaries, from which we can see that the intersection of workspaces for the first and second legs is embodied in the region.

As an example, to present the gross and net rotational capability indices, point O' on the moving platform is specified at point $c(y_c = 0.3, z_c = 2.6)$ in the reachable workspace. The projection of point c to the z- axis is c', as shown in Fig. 11. The circle ν is centered at point c in the plane parallel to plane O-xz and the distance between point c and the z- axis is y_c. The region Ω_3, which is the locus of point P_3 given by (42) when $\rho_3 \in [-3.5, -1.0]$, is shown as Fig. 11. From the figure, we can see that at point c there are two intersecting points, a and b, between ν and $C_{3\max}$ and no intersecting point between ν and $C_{3\min}$. The arc ab is embodied within the region Ω_3. Then the central angle of arc ab is the GRCI, i.e., $\zeta = 183.09^\circ$. As mentioned above, arc ab contains the singular configuration. As shown in Fig. 11, when the third leg is in the configuration of B_3b', i.e., the third leg is in the moving platform plane, the second type of singularity occurs. Therefore, the central angle of arc ab' can be the NRCI, i.e., $\varsigma = 63.31^\circ$ at point c. This is, actually, the NRCI of the manipulator with the assembling mode as shown in Fig. 1.

From Fig. 11, one can see that the central angle of arc bb' is much bigger than that of arc ab'. This characteristic is always right because of the shape and position of $\nu, C_{3\min}$, and $C_{3\max}$, as shown in Figs. 7 and 11. Actually, the central angle of arc bb' represents configurations when the sign "$\pm$" in (7) is "+", and that of arc ab' for those when the sign is "$-$". These configurations correspond to different assembling modes. One can conclude that the former assembling mode has higher rotational capability than the latter one.

If we focus our attention on the assembling mode as shown in Fig. 1, from Fig. 11 we can see that it is easier to reach a singular configuration for the moving platform when $\phi > 0$ than that when $\phi < 0$, for which we can specify the z-coordinate of the joint point B_3 on the third leg to be different from those of the first and second legs. This specification will improve the NRCI. For example, if we adjust from $z = 0$ to $z = 0.4$ for joint point B_3, the NRCI of the point $(y_c = 0.3, z_c = 2.6)$ will be

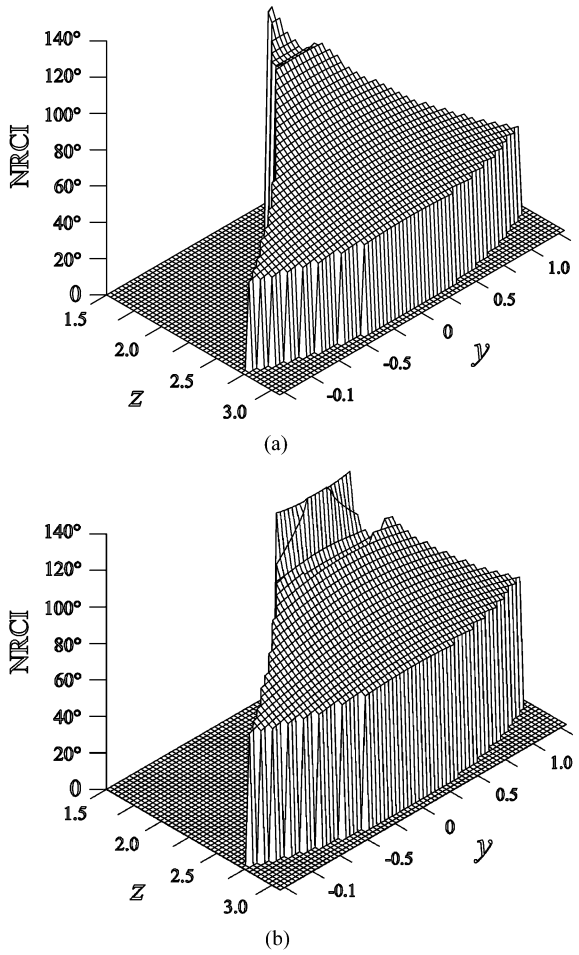

Fig. 12. Distribution of NRCI on the workspace for the example in Section VII. (a) Without modification to the point B_3. (b) after the modification to the point B_3.

$\varsigma = 83.31^\circ$. Note that this modification will result in a different workspace. However, it is very useful for the actual design of the manipulator to increase the rotational capability in the working space of such a device. The GRCI is actually the sum of NRCIs for all assembling modes.

Fig. 12(a) represents the NRCI distribution on the reachable workspace for the manipulator with the assembling mode when the sign "$\pm$" in (7) is "–", which shows the following.

- The NRCI is symmetric about $y = 0.0$.
- The maximum value of ς can reach 129.16°, and the minimum value is 47.50°.

Therefore, the rotational capability of the manipulator can be very good. The NRCI distribution for the manipulator with another assembling mode can be obtained as well, but will not be shown here due to limited space.

Fig. 12(b) shows the distribution of the assembling mode after the modification of z-coordinate for the joint point B_3 from $z = 0$ to $z = 0.4$. The maximum value of ς can reach 139.82°, and the minimum value can reach 71.23°. Therefore, if the third leg is different from the first and second legs the index could be better. But from Fig. 12, one can notice that the workspace is a little different. Practically, the reduced workspace is not used.

VIII. Conclusion

In this paper, a type of new spatial three-DoF parallel manipulator with three nonidentical chains is developed. The movable platform has three DoFs, which are two translations and one rotation, with respect to the base plate. The advantages of the parallel manipulator are as follows: 1) only single-DoF joints; 2) combining spatial translational and rotational degrees of freedom in a spatial three-DoF parallel manipulator; and 3) high rotational capability of the rotational DoF. Both the inverse and forward kinematics problems for the manipulator are described in closed forms. The results show that there can be as many as four solutions for inverse kinematics and four for forward kinematics. The velocity equation of the new parallel manipulator is given. And three kinds of singularities are presented. The workspace of the manipulator is analyzed and the analysis shows that the intersection of reachable workspaces of the first and second legs is the reachable workspace of the parallel manipulator. Rotational capability indices of the manipulator are defined, and the analysis shows that the manipulator has high rotational capability. The parallel manipulator has wide application in the fields of industrial robots, simulators, micromanipulators, and parallel kinematics machines.

References

[1] K. Cleary and T. Brooks, "Kinematics analysis of a novel 6-DOF parallel manipulator," in *Proc. IEEE Int. Conf. Robotics and Automation*, vol. 1, May 1993, pp. 708–713.

[2] S. E. Salcudean *et al.*, "A six degree-of-freedom, hydraulic, one person motion simulator," in *Proc. IEEE Int. Conf. Robotics and Automation*, vol. 3, May 1994, pp. 2437–2443.

[3] D. R. Kerr, Analysis, "Properties and design of Stewart platform transducer," *Trans. ASME, J. Mech. Transm. Automn. Des.*, vol. 111, no. 1, pp. 25–28, 1989.

[4] C. Reboulet and R. Pigeyre, "Hybrid control of a 6-DOF in-parallel actuated micro-manipulator mounted on a Scara robot," in *Proc. Int. Symp. Robotics and Manufacturing: Research, Education and Applications*, vol. 3, Jul. 1990, pp. 293–298.

[5] X.-J. Liu, J. Wang, and F. Gao, "Design for 6-DOF parallel microrobotics mechanisms," *J. Tsinghua Univ. (Sci. Technol.)*, vol. 41, no. 8, pp. 16–20, Aug. 2001.

[6] M. Zhao *et al.*, "Development of an advanced manufacturing system based on parallel robot manipulators," in *Proc. 27th Int. Symp. Robotics*, Apr./May 1998, pp. 96–100.

[7] F. Behi, "Kinematics analysis for a six-degree-of-freedom 3-PRPS parallel manipulator," *IEEE J. Robot. Autom.*, vol. 4, no. 5, pp. 561–565, Oct. 1988.

[8] J. Hudgens and D. Tesar, "A fully-parallel six degree-of-freedom micromanipulator: Kinematics analysis and dynamic model," in *Proc. 20th Biennial ASME Mechanisms Conf.*, Sep. 1988, pp. 29–38.

[9] X.-J. Liu, J. Wang, F. Gao, and L.-P. Wang, "The mechanism design of a simplified 6-DOF 6-RUS parallel manipulator," *Robotica*, vol. 20, no. 1, pp. 81–91, Jan. 2002.

[10] A. Austad, "Arm device," IPN No. WO 87 03239, Jun. 1987.

[11] D. J. Cox and D. Tesar, "The dynamic modeling and command signal formulation for parallel multi-parameter robotic devices," Internal Rep. CIMAR, Univ. Florida, Gainesville, Sep. 1981.

[12] J. Kim *et al.*, "Eclipse-II: A new parallel mechanism enabling continuous 360-degree spinning plus three-axis translational motions," *IEEE Trans. Robot. Autom.*, vol. 18, pp. 367–373, 2002.

[13] T. Huang, X. Zhao, and D. J. Whitehouse, "Stiffness estimation of a tripod-based parallel kinematic machine," *IEEE Trans. Robot. Autom.*, vol. 18, no. 3, pp. 50–58, Jun. 2002.

[14] C. M. Gosselin, S. Lemieux, and J.-P. Merlet, "A new architecture of planar three-degrees-of-freedom parallel manipulator," in *Proc. IEEE Int. Conf. Robotics and Automation*, vol. 4, Apr. 1996, pp. 3738–3743.

[15] L. Slutski, D. Chablat, and J. Angeles, "The kinematics of manipulators built from closed planar mechanisms," in *Proc. IEEE/ASME Int. Conf. Advance Intelligent Mechatronics*, Sep. 1999, pp. 531–536.

[16] R. Clavel, "DELTA: A fast robot with parallel geometry," in *18th Int. Symp. Industrial Robot.*, Apr. 1988, pp. 91–100.

[17] J. M. Hervé, "Group mathematics and parallel link mechanisms," in *IMACS/SICE Int. Symp. Robotics, Mechatronics, and Manufacturing Systems*, Sep. 1992, pp. 459–464.

[18] X.-J. Liu, Z.-L. Jin, and F. Gao, "Optimum design of 3-DOF spherical parallel manipulators with respect to the conditioning and stiffness indices," *Mech. Mach. Theory*, vol. 35, no. 9, pp. 1257–1267, Sep. 2000.

[19] R. D. Gregorio, "A new family of spherical parallel manipulators," *Robotica*, vol. 20, no. 4, pp. 353–358, Aug. 2002.

[20] K. H. Hunt, "Structural kinematics of in-parallel-actuated robotarms," *Trans. ASME, J. Mech., Transm., Automn. Des.*, vol. 105, no. 4, pp. 705–712, Mar. 1983.

[21] B. Siciliano, "The Tricept robot: Inverse kinematics, manipulability analysis and closed-loop direct kinematics algorithm," *Robotica*, vol. 17, no. 4, pp. 437–445, Jul. 1999.

[22] L. W. Tsai, G. C. Walsh, and R. E. Stamper, "Kinematics of a novel three dof translational platform," in *Proc. IEEE Int. Conf. Robotics and Automation*, vol. 4, Apr. 1996, pp. 3446–3451.

[23] M. Ceccarelli, "A new 3 D.O.F. spatial parallel mechanism," *Mech. Mach. Theory*, vol. 32, no. 8, pp. 895–902, Aug. 1997.

[24] X.-J. Liu, Q.-M. Wang, and J. Wang, "Kinematics, dynamics and dimensional synthesis of a novel 2-DoF translational manipulator," *J. Intell. Robot. Syst.*, vol. 41, no. 4, pp. 205–224, Jan. 2005.

[25] C. M. Gosselin and J. Angeles, "Singularity analysis of closed loop kinematic chains," *IEEE Trans. Robot. Autom.*, vol. 6, no. 3, pp. 281–290, Jun. 1990.

[26] H. R. M. Daniali, P. J. Zsombor-Murray, and J. Angeles, "Singularity analysis of a general class of planar parallel manipulators," in *Proc. IEEE Int. Conf. Robotics and Automation*, vol. 2, May. 1995, pp. 1547–1552.

[27] C. M. Gosselin, "Determination of the workspace of 6-DOF parallel manipulators," *ASME J. Mech. Des.*, vol. 112, no. 3, pp. 331–336, Sep. 1990.

[28] I. A. Bonev and J. Ryu, "A new approach to orientation workspace analysis of 6-DOF parallel manipulators," *Mech. Mach. Theory*, vol. 36, no. 1, pp. 15–28, Jan. 2001.

[29] J.-P. Merlet, "Determination of 6D workspace of Gough-type parallel manipulator and comparison between different geometries," *Int. J. Robot. Res.*, vol. 18, no. 9, pp. 902–916, Oct. 1999.

[30] H. K. Tonshoff and H. Grendel, "A systematic comparision of parallel kinematics," in *Parallel Kinematic Machines*, C. R. Boer, L. Molinari-Tosatti, and K. S. Smith, Eds. London, U.K.: Springer-Verlag, 1999, pp. 295–311.

[31] J.-P. Merlet, "The importance of optimal design for parallel structures," in *Parallel Kinematic Machines*, C. R. Boer, L. Molinari-Tosatti, and K. S. Smith, Eds. London, U.K.: Springer-Verlag , 1999, pp. 99–110.

[32] A. G. Chrisp and N. N. Z. Gindy, "Parallel link machine tools: Simulation, workspace analysis and component positioning," in *Parallel Kinematic Machines*, C. R. Boer, L. Molinari-Tosatti, and K. S. Smith, Eds. London, U.K.: Springer-Verlag, 1999, pp. 245–256.

[33] P. Wenger and D. Chablat, "Design of a three-axis isotropic parallel manipulator for machining applications: The Orthoglide," in *Proc. Workshop Fundamental Issues and Future Research Directions for Parallel Mechanisms and Manipulators*, Quebec, QC, Canada, Oct. 2002, pp. 16–24.

[34] X.-J. Liu, J. Jeong, and J. Kim, "A three translational DoFs parallel cube-manipulator," *Robotica*, vol. 21, no. 6, pp. 645–653, Dec. 2003.

[35] B. M. St-Onge and C. M. Gosselin, "Singularity analysis and representation of the general Gough-Stewart platform," *Int. J. Robot. Res.*, vol. 19, no. 3, pp. 271–288, Mar. 2000.

[36] F. C. Park and J. W. Kim, "Singularity analysis of closed kinematic chains," *J. Mech. Des.*, vol. 121, no. 1, pp. 32–38, Mar. 1999.

[37] J.-P. Merlet, C. M. Gosselin, and N. Mouly, "Workspaces of planar parallel manipulators," *Mech. Mach. Theory*, vol. 33, no. 1, pp. 7–20, Jan. 1998.

[38] E. Ottaviano and M. Ceccarelli, "Optimal design of CA-PAMAN (cassino parallel manipulator) with prescribed orientation workspace," *Robotica*, vol. 20, no. 2, pp. 159–166, Mar. 2002.

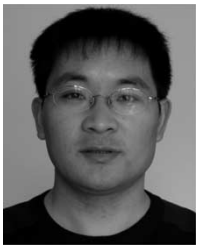

Xin-Jun Liu received the B.S. and M.S. degrees in mechanical design and manufacturing from Northeast Heavy Machinery Institute, Qinhuangdao, China, in 1994 and 1996, respectively, and the Ph.D. degree in mechanical engineering from Yanshan University, Qinhuangdao, China, in 1999.

Currently, he is an Associate Professor in the Department of Precision Instruments at Tsinghua University, Beijing, China. From 2000 to 2001, he was a Postdoctoral Researcher at Tsinghua University. He was a Visiting Researcher at Seoul National University, Seoul, Korea, in 2002–2003. He was an Alexander von Humboldt Research Fellow at the University of Stuttgart, Germany from 2004 to 2005. His research interests include parallel mechanisms, micro-manipulators, parallel kinematic machines, and motion simulators.

Dr. Liu received the Best Youth Paper Award from the IEEE/Control Systems Society, Beijing Chapter, and the Excellent Postdoctoral Fellow Award from Tsinghua University in 2002.

Jongwon Kim received the B.S. degree in mechanical engineering from Seoul National University, Seoul, Korea, in 1978, the M.S. degree from the Korea Advanced Institute of Science and Technology, Daejeon, Korea, in 1980, and the Ph.D. degree from the University of Wisconsin, Madison, in 1987.

He is currently a Professor in the School of Mechanical and Aerospace Engineering, Seoul National University. He has also been a Senior Manager at Daewoo Heavy Industries, Ltd. His research interests are in intelligent manufacturing systems and parallel kinematic machines.

Dr. Kim received the Best Paper Award from the ASME Manufacturing Engineering Division in 1997 and the Society of Manufacturing Engineers University LEAD Award in 1996.